

LHC results and hadronic interaction models

S. Ostapchenko

*Frankfurt Institute for Advanced Studies, 60438 Frankfurt am Main, Germany and
D.V. Skobel'syn Institute of Nuclear Physics, Moscow State University, 119992 Moscow, Russia*

The present status of high energy cosmic ray interaction models is discussed, concentrating on recent model updates inspired by the data from Run 1 of the LHC. A special attention is devoted to the remaining differences in the model predictions and their relation to the underlying theoretical approaches. Opportunities for the model discrimination by future LHC and cosmic ray experimental studies are analyzed.

I. INTRODUCTION

Modeling of high energy hadronic interactions is of considerable importance for experimental studies of very high energy cosmic rays (CRs), especially, for an analysis of the primary CR composition. Applying the traditional extensive air shower (EAS) techniques, i.e. inferring the properties of the primary CR particles from measured characteristics of nuclear-electromagnetic cascades induced by their interactions in the atmosphere, the different primaries are discriminated based on the respective differences between some basic air shower observables, which in turn depend on the way those particles interact with air nuclei.

There are two main experimental procedures [1, 2]. When studying the longitudinal EAS development by measuring fluorescence light produced by excited air molecules, the primary particle type may be inferred from the measured position of the shower maximum X_{\max} – the depth in the atmosphere (in g/cm²) where the number of ionizing particles reaches its maximal value. Remarkably, X_{\max} depends strongly on the properties of the primary particle interaction with air nuclei, notably, on the inelastic cross section and the forward spectra of secondary hadrons produced. Thus, here one may expect to profit maximally from experimental studies of proton-proton and proton-nucleus collisions at the Large Hadron Collider (LHC). On the other hand, when studying air showers with scintillation detectors positioned at ground, the primary particle type is inferred from the relative fraction of muons, compared to all charged particles at ground. As the EAS muon content is formed in a multi-step cascade process, driven mostly by interactions of secondary pions and kaons with air, the muon density ρ_μ at ground depends strongly on the properties of pion-air collisions over a wide range of energies. In particular, any searches for new physics signals with ground-based EAS detectors should be very challenging since the sensitivity to the properties of the primary particle interaction is considerably weakened by the cascade development.

In the following, we are going to discuss the impact of LHC measurements on the modeling of high energy cosmic ray interactions, concentrating in particular on the remaining differences between the predictions of

the popular hadronic interaction models. We shall compare the results of the most recent versions of the EPOS [3, 4], QGSJET-II [5, 6], and SIBYLL [7, 8] models, which all have been updated using experimental data from Run 1 of the LHC. Additionally, we shall use the QGSJET model [9, 10] which, though being already outdated physics-wise, demonstrated a generally good agreement with the LHC data [11]. Hence, it will be used here to study the range of potential variations of model predictions for X_{\max} , in view of current LHC data. Our primary goals are to analyze the differences between the model results, to trace their origin to the underlying approaches for the treatment of hadronic collisions, implemented in those models, and to propose potential measurements by LHC and cosmic ray experiments, which could be able to discriminate between the alternative approaches.

II. IMPACT OF LHC DATA AND REMAINING DIFFERENCES BETWEEN THE MODEL PREDICTIONS

For all contemporary Monte Carlo generators of high energy hadronic collisions, the qualitative picture behind is the one of quantum chromodynamics (QCD): The interactions are mediated by multiple cascades of partons (quarks and gluons) developing between the projectile and target hadrons or nuclei. There comes the predictive power of the models: Once the treatment of the interaction mechanism is developed and the respective parameters are fixed, based on some set of experimental data, a particular model is able to predict the interaction properties at a higher energy or in a different kinematic range. In particular, changing from proton-proton interaction to the pion-proton case or to proton-nucleus (nucleus-nucleus) collisions implies a change of the initial conditions for those parton cascades, without changing the interaction mechanism itself. Yet the corresponding treatments are largely based on phenomenological approaches: While the perturbative QCD allows one to describe the evolution of “hard” (high transverse momentum p_t) partons, it is of little help for many other important aspects, like the evolution of “soft” (small p_t) partons, the multiple scattering mechanism,

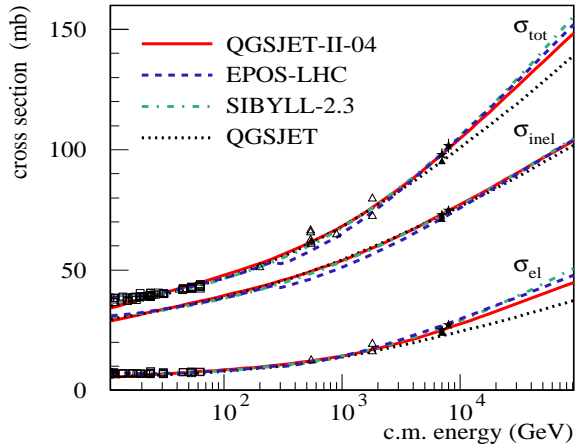


FIG. 1: \sqrt{s} -dependence of the total, inelastic, and elastic pp cross sections, as calculated using the QGSJET-II-04 [6], EPOS-LHC [4], SIBYLL-2.3 [8], and QGSJET [10] models (solid, dashed, dash-dotted, and dotted lines respectively). Experimental data are from Refs. [12–14].

and the very initial conditions for the parton cascades. Therefore, new experimental data corresponding to a different energy or kinematic range are very valuable for tuning the parameters of such phenomenological models and, more importantly, for discriminating invalid theoretical solutions.

In what concerns cosmic ray interaction models, the most important results of Run 1 of the LHC have been precise measurements of the total and elastic proton-proton cross sections by the TOTEM and ATLAS experiments [12, 13]. Apart from reducing drastically the differences between the respective model predictions in the limit of ultra-high energies, as illustrated in Fig. 1, those experimental results constrained a number of key parameters of the models, which impact many other model predictions, e.g. for secondary particle production. While measurements of secondary particle production at the central rapidity region by the ALICE, ATLAS, and CMS experiments at the LHC have not revealed any serious deficiencies of CR interaction models [11], the corresponding experimental results contributed to fine-tuning of model parameters. And the new model versions appeared to be in a reasonably good agreement with experimental data from LHC Run 2 on soft particle production [15–17].

Yet the models diverge considerably in their predictions for EAS properties, as illustrated in Fig. 2 for the particular case of X_{\max} . It is thus highly desirable to reveal the reasons for those differences and to find ways to further constrain model predictions or, even better, to refute some model approaches. In particular, one may hope to gain insight into the problem, based on measurements of forward hadron spectra by the TOTEM and LHCf experiments at the LHC, since the corresponding results proved to be a challenge for most of the present Monte Carlo generators [18–20].

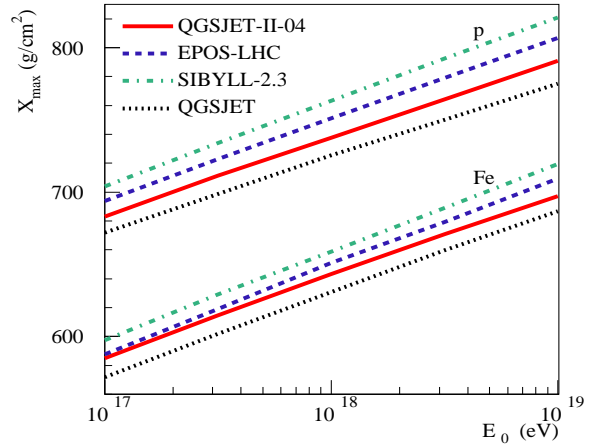


FIG. 2: Primary energy dependence of the average shower maximum depth for proton- and iron-initiated vertical EAS, as calculated using the QGSJET-II-04, EPOS-LHC, SIBYLL-2.3, and QGSJET models (solid, dashed, dash-dotted, and dotted lines respectively).

III. IMPACT OF CONSTITUENT PARTON FOCK STATES

Let us start with SIBYLL-2.3 which predicts the largest values for X_{\max} and for the shower elongation rate between all the considered models, as one can see in Fig. 2. This appears to be related to the very basic model assumptions concerning the structure of constituent parton Fock states in hadrons, i.e. for the above-mentioned initial conditions for parton cascades, as discussed in more detail in Ref. [21]. Like most of the hadronic event generators used in the collider field, the SIBYLL model is based on the “mini-jet” approach which corresponds implicitly to the picture shown schematically on the left-hand side (lhs) of Fig. 3. At large Feynman x , one starts from the same universal parton Fock state. Additional partons (sea quarks or gluons) giving rise to new branches of the parton cascade, which take part in the multiple scattering processes, result from the evolution of the parton density corresponding to this initial state and their momentum fractions are distributed as $\propto 1/x$ in the very high energy limit. Such a picture reflects itself in the hadron production pattern predicted by the model: Multiple scattering affects mostly central particle production, while having a weak influence of forward hadron spectra. Indeed, the latter are formed by the hadronization of partons emerging from the initial part of the underlying parton cascade, which starts from the same initial conditions and covers a short rapidity interval, being thus weakly dependent on the further development of the cascade.

A direct consequence of the above-discussed approach is a weak energy dependence of the inelasticity K^{inel} , i.e. the relative energy loss of leading nucleons,

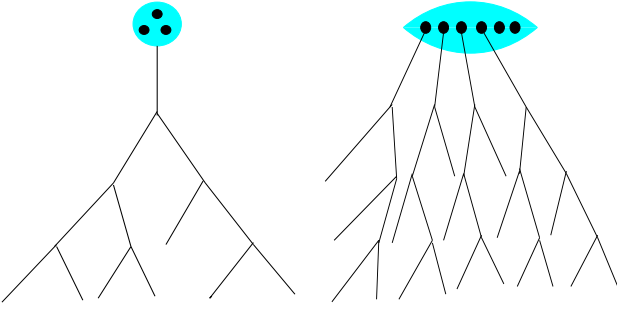


FIG. 3: Schematic view of the initial part of the parton cascade in the proton. Left: the cascade starts from the same universal parton Fock state; new partons participating in multiple scattering processes emerge from the cascade development, being characterized by $\propto 1/x$ distributions for the momentum fraction. Right: the proton is represented by a superposition of Fock states consisting of different numbers of large x constituent partons; the more abundant multiple scattering the larger Fock states involved in the process.

in proton-proton and proton-nucleus collisions. With increasing energy, one obtains a significant enhancement of secondary particle production in the central rapidity region only, which has a weak impact on the energy loss of leading nucleons. As one can see in Fig. 4, the energy dependence of K_{pp}^{inel} is indeed almost flat for SIBYLL-2.3. In turn, a slower energy-rise of the inelasticity implies a larger EAS elongation rate and a larger X_{max} at sufficiently high energies (see, e.g. Ref. [22]), as we observed indeed in Fig. 2.

In the alternative approach, implemented in the EPOS and QGSJET(-II) models, a proton is represented by a superposition of a number of Fock states containing different numbers of large x constituent

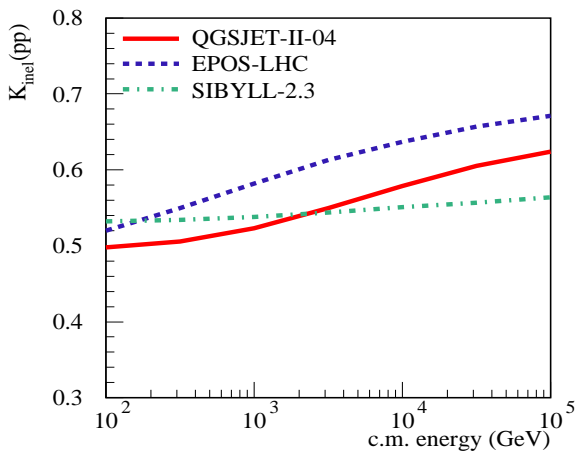


FIG. 4: Energy dependence of the inelasticity of leading nucleons in pp collisions, as calculated using the QGSJET-II-04, EPOS-LHC, and SIBYLL-2.3 models (solid, dashed, and dash-dotted lines respectively).

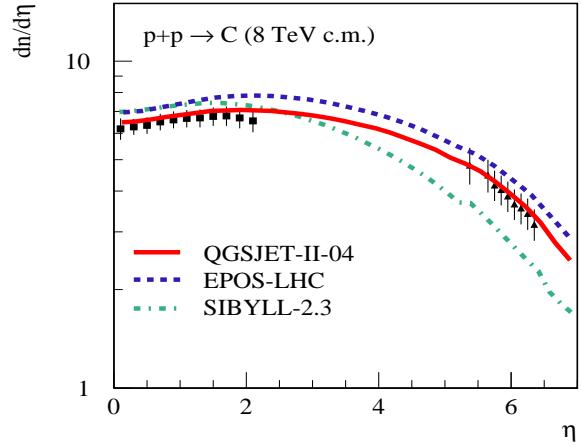


FIG. 5: $d n_{pp}^{\text{ch}}/d\eta$ for pp collisions at $\sqrt{s} = 8$ TeV, as calculated using the QGSJET-II-04, EPOS-LHC, and SIBYLL-2.3 models (solid, dashed, and dash-dotted lines respectively) for the nondiffractive event selection of TOTEM: at least one charged hadron produced both at $-6.5 < \eta < -5.3$ and at $5.3 < \eta < 6.5$. The CMS and TOTEM data are shown by filled squares and filled triangles respectively.

partons, as shown schematically on the right-hand side (rhs) of Fig. 3. Further cascading of these partons “dresses” them with low x parton clouds. As the overall parton multiplicity in the central rapidity region is roughly proportional to the number of initial constituent partons, stronger multiple scattering is typically associated with larger Fock states. Thus, there is a strong long-range correlation between central and forward particle production; higher multiplicity in the central region reflects stronger multiple scattering. In turn, this implies that bigger numbers of large x constituent partons are involved in the process, which has a strong impact on forward hadron spectra.

This naturally leads to a substantial energy-rise of the inelasticity, which is clearly seen in Fig. 4 for QGSJET-II-04 and EPOS-LHC. The reason for this rise is twofold. First, for any given Fock state, increasing multiple scattering implies that bigger numbers of large x constituent partons are involved in the interaction, thus leaving smaller fractions of the initial proton momentum for spectator partons which finally form the leading nucleons. Additionally, Fock states with bigger and bigger numbers of large x constituent partons come into play. Momentum sharing between these partons results in a smaller fraction of the initial proton momentum, possessed by each parton, which thus enhances the energy loss of the leading nucleons.

The minijet approach of the SIBYLL model is already disfavored by recent combined measurements by the CMS and TOTEM experiments of the pseudorapidity η density $d n_{pp}^{\text{ch}}/d\eta$ of produced charged hadrons in pp collisions at $\sqrt{s} = 8$ TeV [18]. As one can see in Fig. 5, $d n_{pp}^{\text{ch}}/d\eta$ predicted by SIBYLL-2.3 steeply falls down at large η , which reflects the quick decrease

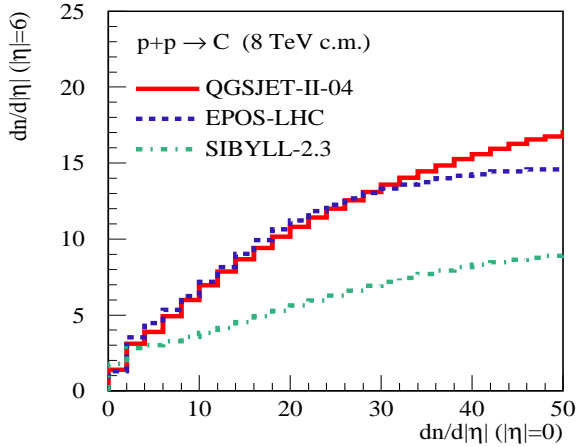


FIG. 6: Pseudorapidity density of produced charged hadrons $dn_{pp}^{\text{ch}}/d|\eta|$ at $|\eta| = 6$ ($p_t > 0$) as a function of $dn_{pp}^{\text{ch}}/d|\eta|$ at $|\eta| = 0$ ($p_t > 0.1$ GeV) in pp collisions at $\sqrt{s} = 8$ TeV, as calculated using the QGSJET-II-04, EPOS-LHC, and SIBYLL-2.3 models (solid, dashed, and dash-dotted lines respectively).

of the number of constituent partons when parton momentum fraction increases. In contrast, EPOS-LHC and QGSJET-II-04 predict a much flatter η -dependence for produced charged hadrons, in a good agreement with the experimental data.

However, the crucial discrimination of the mini-jet approach may be provided measuring correlations between the signal strengths in central and forward-looking detectors at the LHC. For the particular case of the CMS and TOTEM experiments, this is illustrated in Fig. 6, where we plot for $\sqrt{s} = 8$ TeV $dn_{pp}^{\text{ch}}/d|\eta|$ at $|\eta| = 6$ (averaged over the interval $5.5 < |\eta| < 6.5$) as a function of the central η -density ($|\eta| < 1$) of charged hadrons. Both EPOS-LHC and QGSJET-II-04 predict a strong correlation of the signal strengths in CMS and TOTEM. The respective results of the two models practically coincide with each other, apart from the tails of the multiplicity distributions. In contrast, for SIBYLL 2.3 such a correlation is twice weaker, being thus a “smoking gun” signature for the desirable discrimination.

Another possible way for the model discrimination is via measurements of very forward particle production by the LHCf experiment at the LHC, when supplemented by triggering different hadronic activities in ATLAS, as discussed in Ref. [21].

IV. RELEVANCE OF PION-AIR INTERACTIONS

The analysis in Section III does not explain the large, up to 40 g/cm², differences in X_{max} predictions for the other three models which employ essentially the same treatment of constituent parton Fock

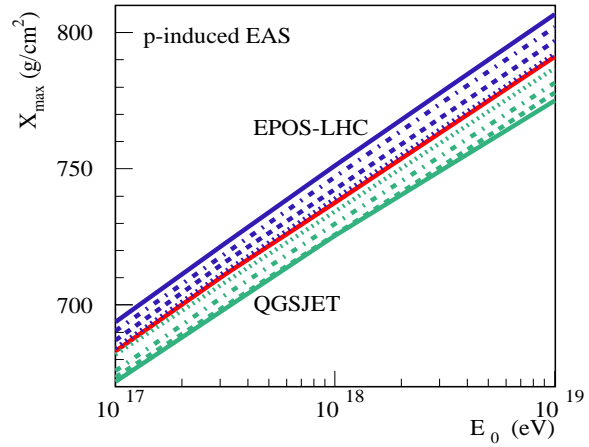


FIG. 7: Primary energy dependence of X_{max} for p -induced vertical EAS, as calculated using the EPOS-LHC, QGSJET-II-04, and QGSJET models (top, middle, and bottom solid lines respectively), or applying mixed model descriptions, as explained in the text (dashed, dash-dotted, and dotted lines).

states. One might relate these differences to present experimental uncertainties concerning the rate of the inelastic diffraction in high energy pp collisions. Indeed, the diffraction has a significant influence on the shape of very forward spectra of secondary hadrons and, through its close relation to the inelastic screening effect, on the calculation of the inelastic proton-air cross section, which in turn both make a strong impact on the longitudinal EAS development. This has been investigated in Ref. [23] in the framework of the QGSJET-II-04 model. The obtained characteristic uncertainty for X_{max} amounted to only 10 g/cm², while being smaller than 3 g/cm² for $\text{RMS}(X_{\text{max}})$.

To reveal the interaction features which are responsible for the remaining differences, one can use the “cocktail” model approach: Using QGSJET-II-04 to describe some selected interactions of hadrons in air showers or some particular features of the primary interaction, while treating the rest with one of the other two models (see Ref. [24] for more details). As the first step, we apply QGSJET-II-04 to determine the position of the primary particle interaction in the atmosphere and to describe the production of secondary nucleons in this interaction, which comprises all the effects of the inelastic diffraction; all other characteristics of the first p -air collision and all the subsequent interactions of secondary hadrons in the cascade are treated using EPOS-LHC. The calculated X_{max} values shown by the upper dash-dotted line in Fig. 7 differ from the original EPOS-LHC results by not more than 5 g/cm², which is well within the uncertainty range obtained in Ref. [23].

Next, we apply QGSJET-II-04 to describe all the characteristics of the primary interaction, while treating the rest of the hadron cascade using EPOS-LHC.

The obtained X_{\max} shown by the upper dashed line in Fig. 7 is shifted further towards the QGSJET-II-04 results by up to 5 g/cm². This additional shift is explained by somewhat harder spectra of secondary hadrons in EPOS-LHC, compared to QGSJET-II-04. We also repeat the same calculation describing secondary hadron interactions in the cascade with the QGSJET model, the results being shown by the lower dashed line in Fig. 7. In this case, the difference with the pure QGSJET-based calculation does not exceed 3 g/cm², which is due to the fact that forward particle spectra in proton-air collisions are rather similar in QGSJET and QGSJET-II-04.

There remains a large difference between the two dashed lines in Fig. 7, which is entirely due to the model treatments of high energy pion-air and kaon-air interactions [24]. The difference between the lower dashed line and the QGSJET-II-04 results is mainly due to the larger pion-air cross section and softer production spectra for secondary mesons in QGSJET, compared to QGSJET-II-04. The former effect is illustrated by the transition from the lower dashed to lower dash-dotted line in Fig. 7 while the latter is responsible for the difference between the lower dash-dotted and dotted lines in the Figure.

In turn, for EPOS-LHC the remaining difference with the QGSJET-II-04 results is due to a copious production of baryon-antibaryon pairs in pion-air and kaon-air collisions, also due to harder (anti-)baryon spectra in EPOS-LHC [25]. This slows down the energy dissipation from the hadronic cascade and thus contributes to the elongation of the shower profile. Indeed, if we apply QGSJET-II-04 to describe both the primary interaction and the production of nucleons and antinucleons in all the secondary pion-air and kaon-air collisions, while treating the rest with EPOS-LHC, the obtained X_{\max} shown by the upper dotted line practically coincides with the QGSJET-II-04 results.

V. RELATION TO MUON PRODUCTION DEPTH

As demonstrated in Section IV, a large part of the model uncertainty for the predicted X_{\max} is related to the treatment of pion-air collisions at very high energies. While there exist no experimental data for such interactions above fixed-target energies, one may try to constrain the models by studying other EAS characteristics. A particularly promising choice is the maximal muon production depth X_{\max}^{μ} in air showers, recently measured by the Pierre Auger Observatory (PAO) [26]. Interestingly, one observed a strong contradiction between the respective EPOS-LHC predictions and the experimental data: The muon production maximum was observed substantially higher in the atmosphere than predicted by that model for

the heaviest possible primary cosmic ray nuclei.

One may generally expect a rather strong sensitivity of the predicted X_{\max}^{μ} to the modeling of pion-air collisions since the EAS muon content is formed in a multi-step hadronic cascade in which the number of pions and kaons increases in an avalanche way until the probability for their decays becomes comparable to the one for interactions. This happens when the energies for most of pions approach the pion critical energy, $E_{\text{crit}}^{\pm} \simeq 80$ GeV. The position of the muon production maximum is close to this turning point.

As a consequence, X_{\max}^{μ} is very sensitive to the forward spectral shape of secondary mesons in pion-air collisions: Producing in each cascade step a meson of a slightly higher energy would mean that a larger number of cascade branching steps is required for reaching the critical energy, with the result that the maximum of the muon production profile will be observed deeper in the atmosphere. On the other hand, a smaller pion-air cross section would increase the pion mean free path and thus also elongate the muon production profile. Actually, a similar effect may be produced by a larger diffractive contribution in pion-air interactions [27]. In addition, in the particular case of the EPOS model, its predictions for X_{\max}^{μ} may be influenced by the copious production of (anti-)baryons in pion-air collisions [25]. Unlike pions and kaons, (anti-)nucleons participate in the hadronic cascade without decays, down to the GeV energy range, producing additional generations of secondary hadrons. Muons emerging from decays of secondary pions and kaons created in interactions of low energy nucleons and antinucleons contribute to the elongation of the muon production profile and give rise to larger values of X_{\max}^{μ} .

Generally, we observe much larger differences between the model predictions for X_{\max}^{μ} , compared to the case of X_{\max} , as demonstrated in Fig. 8. To reveal the reasons for these differences, we use the same “cocktail” model approach as in Section IV. First, we apply QGSJET-II-04 to describe all the characteristics of the primary interaction, while treating the rest of the hadronic cascade using either EPOS-LHC or QGSJET, the results shown respectively by the upper and lower dashed lines in Fig. 8. As expected, the obtained X_{\max}^{μ} values deviate only slightly from the original model calculations – as the model predictions for X_{\max}^{μ} are dominated by the treatment of secondary (mostly pion-air) interactions in the cascade. For example, the smaller X_{\max}^{μ} values predicted by QGSJET are mostly due to somewhat larger inelastic pion-air and kaon-air cross sections and softer meson spectra produced by that model, compared to QGSJET-II-04. The former effect is illustrated by the difference between the lower dashed and dash-dotted lines in Fig. 8, while the latter – by the difference between the lower dash-dotted and dotted lines in the Figure.

In turn, a large part of the difference between EPOS-LHC and QGSJET-II-04 is due to the copious

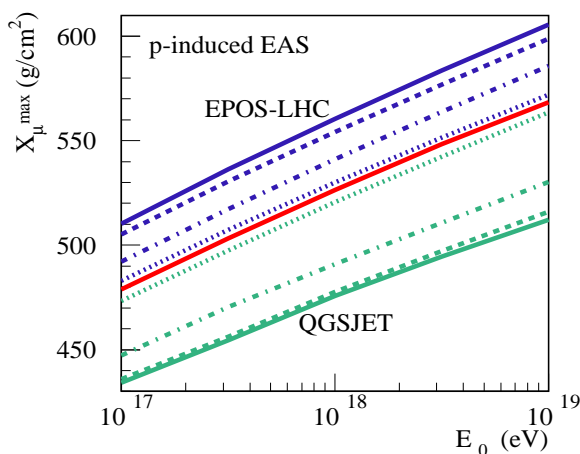


FIG. 8: Primary energy dependence of X_{\max}^{μ} ($E_{\mu} \geq 1$ GeV) for p -induced vertical EAS, as calculated using the EPOS-LHC, QGSJET-II-04, and QGSJET models (top, middle, and bottom solid lines respectively), or applying mixed model descriptions, as explained in the text (dashed, dash-dotted, and dotted lines).

production of baryon-antibaryon pairs in the former model, as illustrated by the transition from the upper dashed to the upper dash-dotted line in Fig. 8. The remaining difference between the two models is mainly due to a larger diffractive contribution in pion-air interactions in EPOS-LHC [27]. Indeed, using QGSJET-II-04 results both for the primary interaction and for hadron spectra in secondary pion-air and kaon-air collisions, we get the energy-dependence of X_{\max}^{μ} , shown by the blue dotted line in Fig. 8, which is very close to the pure QGSJET-II-04 calculation.

Thus, we observed that the same features of pion-air interactions, which had a sizable influence on model predictions for X_{\max} , make a much stronger impact on the corresponding results for X_{\max}^{μ} . This can be used to put strong constraints on the respective model approaches. In particular, the copious production of baryon-antibaryon pairs and the large diffractive contribution in pion-air collisions in EPOS-LHC are clearly disfavored by the PAO data.

VI. MODEL PREDICTIONS FOR $\text{RMS}(X_{\max})$

As already mentioned above, measurements of the total and elastic proton-proton cross sections at the LHC strongly constrained model predictions for fluctuations of the shower maximum position, $\text{RMS}(X_{\max})$, for proton-induced EAS. The remaining uncertainties related to the treatment of inelastic diffraction were estimated to be smaller than 3 g/cm^2 [23]. Comparing in Fig. 9 the respective results of the interaction models tuned to the LHC data, we observe indeed a very good agreement for the case of the primary proton. However, $\text{RMS}(X_{\max})$ for nucleus-

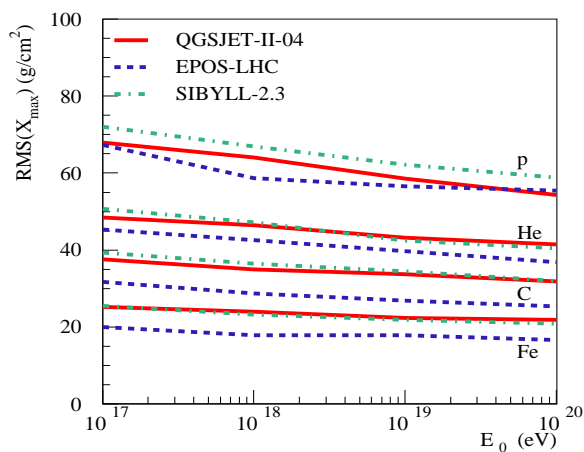


FIG. 9: Primary energy dependence of $\text{RMS}(X_{\max})$ for p -, He-, C-, and Fe-induced vertical EAS, as calculated using the QGSJET-II-04, EPOS-LHC, and SIBYLL-2.3 models (solid, dashed, and dash-dotted lines respectively).

induced air showers is quite sensitive to the treatment of the fragmentation of the nuclear spectator part [9]. Thus, it is quite remarkable that the corresponding predictions of QGSJET-II-04 and SIBYLL-2.3 rather precisely coincide with each other, despite using different modeling of the nuclear breakup. In this respect, the much smaller fluctuations of X_{\max} for nuclear primaries, predicted by EPOS-LHC, are surprising.

To gain further insight into the issue, we compare in Fig. 10 the results of QGSJET-II-04 and SIBYLL-2.3

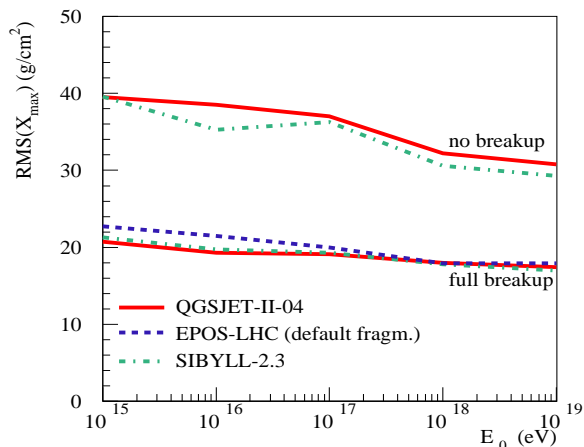


FIG. 10: Primary energy dependence of $\text{RMS}(X_{\max})$ for Fe-induced vertical EAS, calculated with QGSJET-II-04 and SIBYLL-2.3 (solid and dash-dotted lines respectively) for two nuclear breakup options, as discussed in the text, compared to the default EPOS-LHC results (dashed line).

for $\text{RMS}(X_{\max})$ of iron-induced EAS, considering two extreme (and unrealistic) assumptions concerning the nuclear fragmentation: Treating the complete spectator part as a single nucleus (no breakup) or assuming

it to disintegrate into separate nucleons (full breakup). It is easy to see that the latter option gives rise to twice smaller X_{\max} fluctuations, compared to the former, as noticed already in [9], and that the predictions of the two models agree rather precisely with each other, for both scenario. The latter is not surprising since the corresponding results for $\text{RMS}(X_{\max})$ are dominated by fluctuations of the numbers of “wounded” (taking part in the interaction) projectile nucleons, which are defined by the geometry of nuclear collisions in the Glauber-Gribov approach. In contrast, the values of $\text{RMS}(X_{\max})$, obtained with EPOS-LHC for the two above-discussed fragmentation options, coincide within 2 g/cm^2 with each other and with the default model results plotted as the dashed line in Fig. 10. Moreover, the X_{\max} fluctuations predicted by EPOS-LHC are very close to the ones obtained with both QGSJET-II-04 and SIBYLL-2.3, using the full breakup option, which is clearly inconsistent with experimental data on nuclear fragmentation (see, e.g., [28] for a review). It is noteworthy that the above-demonstrated underestimation of X_{\max} fluctuations by EPOS-LHC may bias an analysis of the cosmic ray mass composition.

VII. FEW COMMENTS ON THE PAO MUON EXCESS AND POTENTIAL SIGNALS OF NEW PHYSICS

Let us finally discuss the outstanding puzzle related to the PAO measurements of the EAS muon content: For primary energies around 10^{19} eV, the observed muon density appeared to exceed by a large factor (1.5 – 2) the one predicted by air shower simulations [29, 30]. Potential explanations of such a muon excess are very challenging, keeping in mind that the muon content of air showers is formed in a multistep cascade process, which involves hadron-air interactions over a wide energy range. Hence, it is very difficult to create such an excess at ultra-high energies only, while keeping the simulation results unchanged at lower energies.

To see that, let us assume that there is no serious problem with the predicted EAS muon number N_{μ} up to primary energies $E_0 \sim 10^{17}$ eV, as indicated by experimental data [31–34]. Taking into account that most of secondary hadrons are produced with rather small fractions of the primary particle energy $x_E < 0.1$, there is at most one cascade step before the secondary particle energies fall below 10^{17} eV, for a proton-initiated shower of 10^{19} eV. How strong a modification of the primary interaction is then needed to reproduce the PAO muon excess? If we assume that some potentially new mechanism allows one to enhance the multiplicity of the first interaction by as much as a factor of two, this would result in less than 10% enhancement of N_{μ} at ground level [35].

Let us yet further speculate that some new physics emerges around 10^{19} eV, giving rise to an order of magnitude enhancement of the multiplicity, which should just be sufficient to reach an agreement with the PAO results. For having such a strong effect in average, the new physics should affect most of the primary collisions, rather than a small fraction of those, i.e. to emerge with cross sections comparable to the total inelastic proton-air cross section at those energies, $\sigma_{p\text{-air}}^{\text{inel}} \sim 0.5$ barn. Keeping in mind that dedicated searches for the Beyond-Standard-Model physics at the Large Hadron Collider proceed presently at the femtobarn level, this should be considered as a highly speculative scenario. It is noteworthy that such an option may be discriminated by the Pierre Auger collaboration. Indeed, based on simple geometry arguments, one can conclude that a large contribution to proton-air interactions comes from peripheral (large impact parameter b) collisions, characterized by a small number of “wounded” target nucleons and relatively low parton densities. Such peripheral collisions are thus far from reaching extreme conditions for the new physics to emerge. If we then assume that in some, say, 10% of most central (small b) interactions a “hyper-fireball” is created, producing an order of magnitude higher than average multiplicity, this would give rise to huge event-by-event fluctuations of the muon density at ground, $\delta\rho_{\mu}/\rho_{\mu} > 100\%$. Such an order of magnitude enhancement of $\delta\rho_{\mu}$ can be easily observed by ground detectors.

VIII. OUTLOOK

Experimental studies of proton-proton collisions at the LHC substantially reduced the uncertainties of numerical simulations of CR-induced air showers, notably, thanks to the precise measurements of the total and elastic pp cross sections by the TOTEM and ATLAS experiments. Nevertheless, there exists yet a significant spread between the model predictions for the shower maximum position. The largest between all the models X_{\max} values predicted by SIBYLL-2.3 are due to the very weak energy dependence of the inelasticity of that model, which is a direct consequence of its grounding minijet approach. While that approach is already disfavored by combined studies of particle production by CMS and TOTEM, the final discrimination will be provided by measuring correlations between the signal strengths in central and forward-looking LHC detectors, like CMS and TOTEM, or ATLAS and LHCf.

Apart from such a discrimination and more precise measurements of the inelastic diffraction, the LHC potential for improving EAS simulations is already limited since the dominant source of uncertainties shifts towards the model treatments of very high energy pion-air interactions. This can be constrained indi-

rectly by studying other air shower observables, notably, by measurements of the maximal muon production depth. In particular, the PAO results on X_{\max}^{μ} disfavor the copious production of baryon-antibaryon pairs and the large diffractive contribution in pion-air collisions, predicted by EPOS-LHC. Hence, one may expect that X_{\max} predictions of a corrected version of the model will move closer to the QGSJET-II-04 results.

It is noteworthy that even for QGSJET-II-04 there is a certain tension between the data of the Pierre Auger experiment on X_{\max} and X_{\max}^{μ} [26]: The latter point towards a heavier CR composition, compared to the former. In principle, one may try to reach a consistency between the two results by modifying the treatment of pion-air collisions. However, as the potential changes would impact X_{\max}^{μ} much stronger

than X_{\max} , this would imply to aim at higher inelastic cross section and/or softer hadron production spectra for such interactions, which would push one towards a predominantly light, presumably proton-dominated CR composition. In turn, this would contradict other PAO results [36, 37]. Thus, the situation remains confusing and further progress, both on the experimental and the theoretical sides, is desirable.

Acknowledgments

The author acknowledges the support by Deutsche Forschungsgemeinschaft (Project OS 481/1).

-
- [1] M. Nagano and A. A. Watson, *Rev. Mod. Phys.* **72**, 689 (2000).
 - [2] K.-H. Kampert and M. Unger, *Astropart. Phys.* **35**, 660 (2012).
 - [3] K. Werner, F.-M. Liu, and T. Pierog, *Phys. Rev. C* **74**, 044902 (2006).
 - [4] T. Pierog, Iu. Karpenko, J. M. Katzy, E. Yatsenko, and K. Werner, *Phys. Rev. C* **92**, 034906 (2015).
 - [5] S. Ostapchenko, *Nucl. Phys. Proc. Suppl.* **151**, 143 (2006); *Phys. Rev. D* **74**, 014026 (2006).
 - [6] S. Ostapchenko, *Phys. Rev. D* **83**, 014018 (2011); *EPJ Web Conf.* **52**, 02001 (2013).
 - [7] R. S. Fletcher, T. K. Gaisser, P. Lipari, and T. Stanev, *Phys. Rev. D* **50**, 5710 (1994); E.-J. Ahn, R. Engel, T. K. Gaisser, P. Lipari, and T. Stanev, *ibid.*, **80**, 094003 (2009).
 - [8] F. Riehn, R. Engel, A. Fedynitch, T. K. Gaisser, and T. Stanev, *Proc. Sci., ICRC2015* (2016), 558 [arXiv:1510.00568].
 - [9] N. N. Kalmykov and S. S. Ostapchenko, *Phys. Atom. Nucl.* **56**, 346 (1993).
 - [10] N. N. Kalmykov, S. S. Ostapchenko, and A. I. Pavlov, *Nucl. Phys. Proc. Suppl.* **52B**, 17 (1997).
 - [11] D. d'Enterria, R. Engel, T. Pierog, S. Ostapchenko, and K. Werner, *Astropart. Phys.* **35**, 98 (2011).
 - [12] G. Antchev *et al.* (TOTEM Collaboration), *Europhys. Lett.* **101**, 21002 (2013); *ibid.*, 21003 (2013); *ibid.*, 21004 (2013); *Phys. Rev. Lett.* **111**, 012001 (2013).
 - [13] G. Aad *et al.* (ATLAS Collaboration), *Nucl. Phys. B* **889**, 486 (2014).
 - [14] K. Nakamura *et al.* (Particle Data Group), *J. Phys. G* **37**, 075021 (2010).
 - [15] V. Khachatryan *et al.* (CMS Collaboration), *Phys. Lett. B* **751**, 143 (2015).
 - [16] M. Aaboud *et al.* (ATLAS Collaboration), *Eur. Phys. J. C* **76**, 502 (2016).
 - [17] J. Adam *et al.* (ALICE Collaboration), *Phys. Lett. B* **753**, 319 (2016).
 - [18] S. Chatrchyan *et al.* (CMS and TOTEM Collaborations), *Eur. Phys. J. C* **74**, 3053 (2014).
 - [19] G. Antchev *et al.* (TOTEM Collaboration), *Eur. Phys. J. C* **75**, 126 (2015).
 - [20] O. Adriani *et al.* (LHCf Collaboration), *Phys. Lett. B* **703**, 128 (2011); *ibid.* **715**, 298 (2012); *ibid.* **750**, 360 (2015); *Phys. Rev. D* **86**, 092001 (2012); *ibid.* **94**, 032007 (2016).
 - [21] S. Ostapchenko, M. Bleicher, T. Pierog, and K. Werner, *Phys. Rev. D* **94**, 114026 (2016).
 - [22] R. Ulrich, R. Engel, and M. Unger, *Phys. Rev. D* **83**, 054026 (2011).
 - [23] S. Ostapchenko, *Phys. Rev. D* **89**, 074009 (2014).
 - [24] S. Ostapchenko and M. Bleicher, *Phys. Rev. D* **93**, 051501 (2016).
 - [25] T. Pierog and K. Werner, *Phys. Rev. Lett.* **101**, 171101 (2008).
 - [26] A. Aab *et al.* (Pierre Auger Collaboration), *Phys. Rev. D* **90**, 012012 (2014); *ibid.*, **90**, 039904 (2014); *ibid.*, **92**, 019903 (2015).
 - [27] T. Pierog, EPJ Web Conf. **99**, 09002 (2015); T. Pierog, B. Guiot, and K. Werner, *Proc. Sci., ICRC2015* (2016), 337.
 - [28] S. Fredriksson, G. Eilam, G. Berlad, and L. Bergström, *Phys. Rep.* **144**, 187 (1987).
 - [29] A. Aab *et al.* (Pierre Auger Collaboration), *Phys. Rev. D* **91**, 032003 (2015); *ibid.*, **91**, 059901 (2015).
 - [30] A. Aab *et al.* (Pierre Auger Collaboration), *Phys. Rev. Lett.* **117**, 192001 (2016).
 - [31] W. D. Apel *et al.* (KASCADE Collaboration), *Astropart. Phys.* **24**, 467 (2006).
 - [32] W. D. Apel *et al.* (KASCADE-Grande Collaboration), *Astropart. Phys.* **65**, 55 (2015).
 - [33] Yu. A. Fomin *et al.*, arXiv:1609.05764.
 - [34] J. G. Gonzalez for the ICECUBE Collaboration, *J. Phys. Conf. Ser.* **718**, 052017 (2016).
 - [35] S. Ostapchenko, *Czech. J. Phys.* **56**, A149 (2006).
 - [36] P. Abreu *et al.* (Pierre Auger Collaboration), *JCAP* **1302**, 026 (2013).
 - [37] A. Aab *et al.* (Pierre Auger Collaboration), *Phys. Lett. B* **762**, 288 (2016).